RSC Advances

This article can be cited before page numbers have been issued, to do this please use: L. yan, Y. zhang, G. Ji, L. Ma, J. Chen, B. Xu and W. Tian, *RSC Adv.*, 2016, DOI: 10.1039/C6RA07520G.

ROYAL SOCIETY OF CHEMISTRY

www.rsc.org/advances

View Article Online
DOI: 10.1039/C6RA07520G

Journal Name

ARTICLE

Multifuctional Polymer Nanoparitcles: Ultra Bright Near-infrared Fluorescence and Strong Magnetization and Their Biological Applications

Received 00th January 20xx,
Accepted 00th January 20xx

DOI: 10.1039/x0xx00000x

www.rsc.org/

Lulin Yan, [†a] Yan Zhang , [†a] Guang Ji,[a] Lian Ma,[a] Jinlong Chen,[a] Bin Xu,*[a] Wenjing Tian[a]

Multifunctional polymer nanoparticles with great promise for biomedical applications have attracted many attentions. Using an aggregation-enhanced emission (AEE) molecule DPPBPA and magnetic Fe_3O_4 as the core, and biocompatible polymer Pluronic F-127 as the encapsulation matrix, the multifuctional polymer NPs Fe_3O_4/DPPBPA@F-127 were fabricated by self-assembly procedures. These NPs have bright near-infrared fluorescence λ_{ex} at 654 nm with high fluorescence quantum yield of 18.3%, and strong magnetism, superparamagnetism. With good monodispersity and biocompatibility, the NPs not only can show effective MRI ability, but also can stain in cytoplasm with a strong near-infrared fluorescent signal, as well as little toxicity to living cells, which show a very good prospect in the field of biological applications.

Introduction

Multifunctional nanoparticles (NPs) with unique magnetic, optical, catalytic, and electrical properties have hold great promise for biomedical applications such as drug delivery carriers [1, 2], diagnostic analysis[3], magnetic resonance imaging[4], bioseperation[5], and fluorescent labeling[6], and attracted many attentions in the past decades.[7-11] The combination of magnetic and fluorescent capabilities enables the design of new multifunctional NPs probes in multimodal optical/magnetic resonance imaging.[9-11] Because of the optical transparence and biological compatibility, polymer have become favorable encapsulation matrixes. Furthermore, the encapsulation can protect dye molecules from the external perturbation and prevent the magnetic nanoclusters from agglomerating into large chunks.[12]

To prepare fluorescent magnetic NPs for imaging, the luminescent QDs and organic dyes were both chosen in the past studies. However, QDs are less chemically stable, potentially toxic, and show fluorescence intermittence[13], and most commercially organic dyes typically exhibit rapid photobleaching and a low fluorescence quantum yield in the NPs due to the notorious aggregation-caused quenching (ACQ) effect. Therefore, the luminescent materials with high photo-stability, low optical background and bright light emission are required[14]. Recently, opposite to the ACQ effect, a novel class of organic fluorophores[15-19] with aggregation-induced emission (AIE) characteristic has been developed. These fluorophores almost have no emission in their dilute solutions, but have high fluorescence quantum yields in the aggregate state when the intramolecular rotations are restricted[15]. These AIE fluorophores opened a new gate to fabricate high brightness NPs by encapsulating large amount of dyes.

Due to the superparamagnetism, nontoxicity, and biodegradability, magnetic iron oxide NPs have become famous magnetic materials.[20] However, as we know, when the fluorescent material cones in contact with iron oxide, most of the fluorescence is quenched.[21, 22] For the AIE characters, the NPs fabricated by combining AIE dyes and iron oxide may overcome this problem. In order to get both high fluorescence quantum yields and strong magnetism in the aggregate state, Tang and co-workers succeeded in synthesizing silica NPs with both efficient fluorescence and strong magnetization by using AIE dyes and iron oxide firstly.[12] And then, some other AIE fluorescent magnetic NPs have been developed.[23-26] However, most of these dyes are blue or green emitters[15, 27-29], whose fluorescence is still quenched to some extent by the magnetic materials, expecially iron oxide, and the intensity of magnetism is always weak, which are not ideal for imaging applications. Because of the low photodamage, deep tissue penetration and minimal auto-fluorescence from biological substrates, the fluorophores with intense emission in the far red/near-infrared (FR/NIR) (650–900 nm) region have attracted much interest[30-32]. Up to now, the investigations about AIE dyes applied in near-infrared emission bioimaging are just emerged, [32-36] and the reports on NPs with both bright

[a] State Key Laboratory of Supramolecular Structure and Materials, Jilin University, Changchun, 130012, P. R. China. E-mail: xubin@jlu.eu.cn

† These authors contributed equally to this work and should be considered co-first authors.

Electronic Supplementary Information (ESI) available: [details of any supplementary information available should be included here]. See DOI: 10.1039/x0xx00000x

View Article Online
DOI: 10.1039/C6RA07520G

FR/NIR fluorescence and strong magnetism are quite limited.[26]

Here, we present a simple strategy to fabricate multifunctional polymer NPs Fe_3O_4/DPPBPA@F-127, by using oleic acid coated magnetic Fe_3O_4 (OA-Fe_3O_4) and an AEE molecule (2Z, 2'Z)-3, 3'-(2, 5-di (piperidin-1-yl)-1, 4-phenylene) bis (2-phenylacrylonitrile) (DPPBPA) as the core, and biocompatible polymer Pluronic F-127 as the encapsulation matrix. During the nanoparticle formation, OA-Fe_3O_4 and DPPBPA tended to entangled with the hydrophobic domains of Pluronic F-127 to afford the hydrophobic interiors, while the hydrophilic domains of Pluronic F-127 extended into the aqueous phase, which makes the NPs stable in the aqueous suspension. With very little fluorescence quenching and magnetic intensity reducing, these NPs possess bright near-infrared fluorescence (λ_{ex} = 654 nm, Φ_f = 18.3%), strong magnetism (Ms = 35.66 emu/g) and superparamagnetism (Mr = 0.3186 emu/g, Hci = 6.377 G), which show that the goals to prepare nanostructureed materials with high near-infrared fluorescence efficency and magnetic susceptibility have been achieved. And these NPs are expected to facilitate their biological applicataions.

Results and Discussion

Synthesis of DPPBPA and oleic acid coated Fe_3O_4 (OA- Fe_3O_4)

The synthetic route to DPPBPA is shown in **Scheme S1**. (2Z,2'Z)-3,3'-(2,5-dibromo- 1,4-phenylene)bis(2-phenylacrylonitrile) (**2**) was synthesized by coupling 2,5-Dibromobenzene -1,4-dicarbaldehyde (**1**) and benzyl cyanide through Knoevenagel reaction[37]. Under typical Suzuki reaction conditions, the target molecule was derived from connect piperidine to the 2,5-positions of compound **2** [38]. All compounds were characterized by standard spectroscopic methods, from which satisfactory analysis data corresponding to their molecular structures were obtained. The molecular structure and purity were confirmed by ^{1}HNMR and MS (**Figure S1** and **S2** in the Supporting Information), which all gave satisfactory spectroscopic data. The final product gives a $[M + H]^+$ peak at m/z 498 (calcd: 498.66) in the GC-MS spectra for DPPBPA, confirming the formation of the expected adducts.

After the synthesis of AEE dye DPPBPA, we then worked on the preparation of magnetic particles. Among various magnetic materials, the Fe_3O_4 particles become a good candidate, since its biocompatibility and wide biological applications such as magnetic resonance imaging, enzyme and protein immobilization. The Fe_3O_4 particles were prepared by a coprecipitation method with oleic acid as stabilizer[39]. Ferric chloride hexahydrate and ferrous chloride tetrahydrate was dissolved in deionized (DI) water with the radio of 2:1. Potassium oleate and ammonium hydroxide was added into the solution at 80 ^oC. The OA-Fe_3O_4 magnetic NPs were centrifuged by supercentrifuge[10]. The oleic acid coated iron oxide retained the characteristic X-ray diffraction pattern of Fe_3O_4 at 2θ of 30.2, 35.5, 43.2, 53.3, 57.1, and 62.8 as listed in ASTM XRD standard card (19-0629) (as shown in **Figure S3,** green line). A transmission electron microscopy (TEM) image showed a mean size of OA-Fe_3O_4 particles of 10 nm in diameter (**Figure 2A**), which indicates that these particles are monodisperse. The magnetic NPs were dispersed in THF at 10 mg/mL for further study.

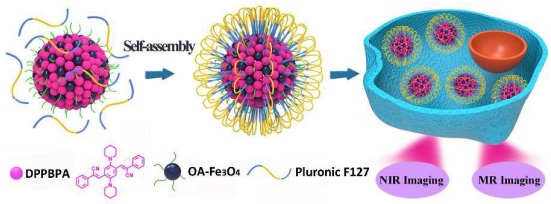

Scheme 1. Schematic illustration of chemical formation of Fe_3O_4/DPPBPA@F127

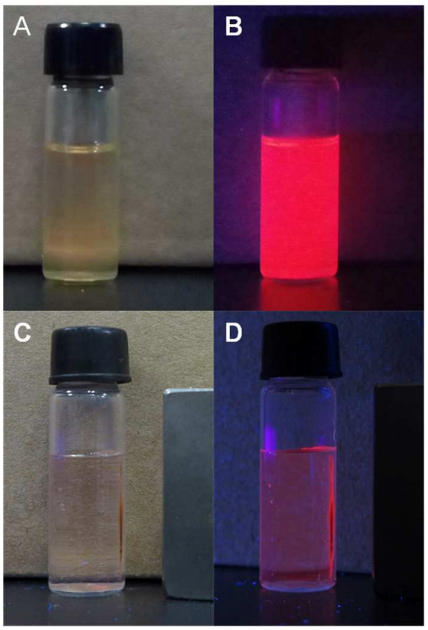

Figure 1. Photographs of water solutions of Fe_3O_4/DPPBPA@F127 taken under A–C) normal room lighting and B–D) UV illumination in the absence (A and B) and presence (C and D) of external magnetic field from a bar magnet.

Nanoparticle preparation and Characterization

As shown in **Scheme 1,** the multifunctional polymer NPs Fe_3O_4/DPPBPA@F-127 were fabricated by a self-assembly procedure, where magnetic OA-Fe_3O_4 and DPPBPA served as the core, and biocompatible polymer Pluronic F-127 served as the encapsulation matrix[40]. Pluronic F127 is a copolymer consisting poly (ethylene oxide)–poly (propylene oxide)–poly (ethylene oxide) blocks, PEO_{100}-PPO_{65}–PEO_{100}. The exterior PEO corona provides an antifouling character to prevent aggregation, protein adsorption, and recognition by the reticulo-endothelial system (RES) and the hydrophobic PPO core can be adapted to encapsulate the fluorophores. The self-assembling characteristics of F127 have been extensively explored in the form of micelles. OA-Fe_3O_4, DPPBPA and Pluronic F-127 were dispersed in THF by a vigorous bath sonicator. The solution mixture was quickly added into DI

View Article Online
DOI: 10.1039/C6RA07520G

water in a vigorous bath sonicator. The THF was removed by nitrogen stripping. The solution was concentrated by continuous nitrogen on a 90 ºC hotplate followed by filtration through a 0.2 micron filter[41]. During the formation procedure of the NPs, the OA-Fe_3O_4 and DPPBPA tended to entangle with the hydrophobic domains of Pluronic F-127 and afford the hydrophobic interiors, while the hydrophilic domains of Pluronic F-127 extend into the aqueous phase of the NPs.

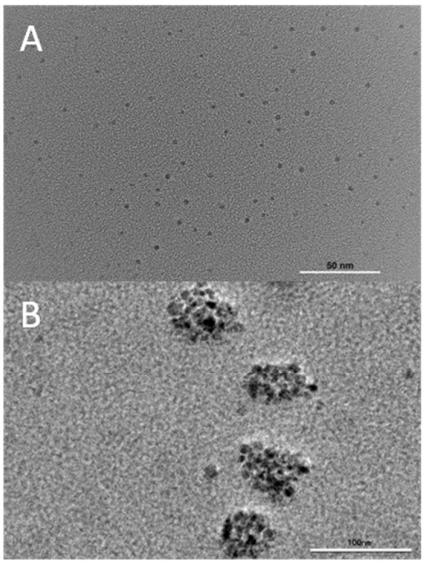

Figure 2. TEM image of OA-Fe_3O_4(A) and Fe_3O_4/DPPBPA@F127(B).

In order to optimize the size and morphology of the NPs, many parameters should be taken into account. As the previous studies, the sizes of the polymer NPs are affected by the amount of polymer added. Under the condition shown in **Table S1**, the NPs are formed with four different polymer amount (mass of polymer: 6 mg, 8 mg, 10 mg, 12 mg). The number average hydrodynamic diameters of the nanoparticle are around 90-105 nm, and the NPs possess the uniform size and monodisperse confirmed by dynamic light scattering (DLS) , which show a narrow peak in the size distribution diagram, as shown in **Figure S4**. Notably, when the addition amount of polymer increase to 10 mg, the encapsulated NPs show the narrowest peak and maximum yield. Therefore, we choose the addition amount of polymer at 10 mg to further fabricate the multifunctional polymer NPs. Zeta potential analyses reveal that the Fe_3O_4/DPPBPA@F-127 NPs possess appreciable surface charges and hence good colloidal stability, which shows a negative charge of around −12.5 mV due to the protonation of oxygen atom in the Pluronic F-127. These negative charges on the surface will stabilize the NPs in aqueous medium by electrostatic repulsion (**Figure S5**). According to the TEM, the average diameter of the NPs is about 65 nm. This size is smaller than that of NPs obtained by DLS analysis due to the shrinkage of the outer hydrophilic chains of Fe_3O_4/DPPBPA@F-127, which often occur under the high vacuum in the TEM chamber.

Photophysical Properties

The images in **Figure 1** show that the suspension of Fe_3O_4/DPPBPA@F-127 in water exhibit good dispersion in the solutions and can be attracted by a bar magnet. The intense near-infrared light was observed in the suspension solution of Fe_3O_4/DPPBPA@F-127 with and without magnet upon the UV illumination[12]. It indicates that both DPPBPA and OA-Fe_3O_4 were suceessfully encapsulated into the NPs. The fluorescence quantum yield (Φ_f) of Fe_3O_4/DPPBPA@F-127 NPs is surprisingly as high as 18.3%. Compared with our previous report, the fluorescence quantum yield of DPPBPA@F-127 NPs without Fe_3O_4 encapsulated is 20% (**Table S2**).[42] This means that there is alomost no quenching of fluorescence when the Fe_3O_4 co-encapsulated together with DPPBPA.

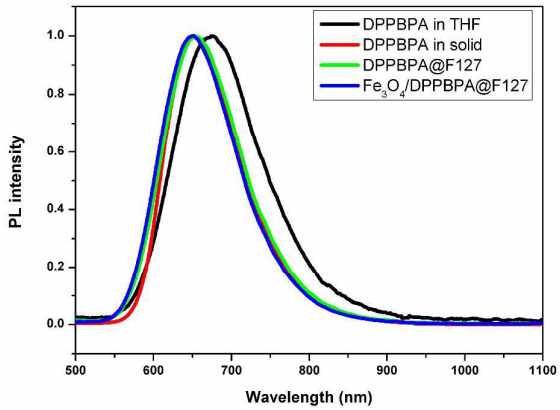

Figure 3. Normalized PL spectra of DPPBPA and NPs.

To get indepth understanding of emission behavior of the Fe_3O_4/DPPBPA@F-127 NPs, we check the effect of both DPPBPA and OA-Fe_3O_4 loading amounts (**Table 1**). With enlarging the loading amount of DPPBPA from 0.5 mg to 1 mg, the fluorescence quantum yield can increase. On the contrary, the fluorescence quantum yield shows obvious decrease when adding more OA-Fe_3O_4 particles. Although the combination of luminescent dye and magnetic particles often quench the fluorescence, the high quantum yield of these NPs can be achieved, even that a low dye loading was used for the nanoparticle fabrication and relative high loading of OA-Fe_3O_4 in the polymer NPs. It is well known that the luminescent dyes with AIE or AEE active have the enhancement emission in their aggregated states, which originate from the restriction of intramolecular rotations (RIR). The properties of enhancement emission is mainly affected by the aggregate state and quite different from the traditional luminescence process, such as fluorescence resonance energy transfer (FRET) [43]or photoinduced electron transfer (PET)[44, 45], which often accompanied by the electronic process in the excited state of luminescent dye. Therefore, we infer that the extraordinary emission properties of these NPs are probably caused by less interaction between the excited state of the DPPBPA and magnetic Fe_3O_4.

View Article Online
DOI: 10.1039/C6RA07520G

Table 1. The fluorescent quantum yield(Φ_f) and spinlattice relaxation time T_1 with different content of DPPBPA and Fe_3O_4

	DPPBPA	OA-Fe_3O_4	F127	THF	H_2O	Φ_f	$1/T_1(S^{-1})$
1	0.5mg	1mg	10mg	5mL	15mL	16.4%	
2	1mg	1mg	10mg	5mL	15mL	18.3%	0.24
3	0.5mg	2mg	10mg	5mL	15mL	7%	
4	1mg	2mg	10mg	5mL	15mL	14%	0.30

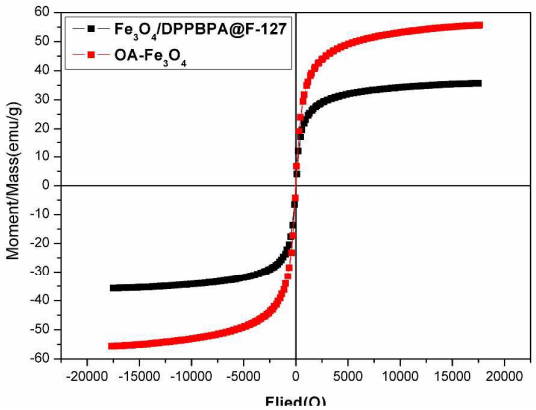

Figure 4. Plots of magnetization versus applied magnetic field at 300 K for OA-Fe_3O_4 and Fe_3O_4/DPPBPA@F127.

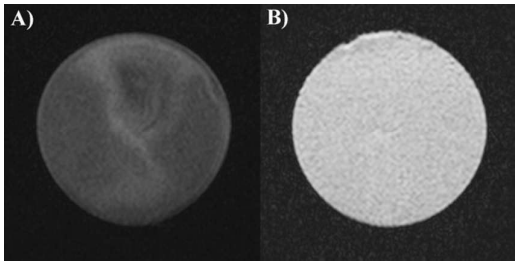

Figure 5. MRI results of A) water and B) Fe_3O_4/DPPBPA@F127

DPPBPA is a typical AEE active luminogen, which show weak near-infrared emission peaked at 674 nm in its THF solution, and strong emission located at 654 nm in the solid state with high quantum yield (Φ_f = 78%). The emission spectra of Fe_3O_4/DPPBPA@F-127 and DPPBPA@F-127 NPs are almost same and with the peak located at 654 nm under the same measurement conditions, which are similar with the emission spectrum in solid state (**Figure 3**). The fluorescence quantum yield of Fe_3O_4/DPPBPA@F-127 shows slight decrease compared with that of DPPBPA@F-127. In addition, time resolved fluorescence spectra of Fe_3O_4/DPPBPA@F-127 and DPPBPA@F-127 NPs shown in **Figure S6** reveals the similar fluorescence lifetime τ_{FL} of both systems, 8.25 ns for Fe_3O_4/DPPBPA@F-127 and 8.63 ns for DPPBPA@F-127, respectively. Since Φ_f equals the product of τ_{FL} and radiative deactivation rate (k_r) , k_r and non-radiative deactivation rate (k_{nr}) can be approximately estimated as listed in Table S2. It shows obviouly that the radiative deactivation process of exicted state have not be affected when the magnetic OA-Fe_3O_4 particles added, which is in agreement with the observation of high solid state fluorescence quantum yield. Furthermore, the flourescence is so stable that there was nearly no change in the spectrum, after put on shelves for several weeks without protection from light and air. The leaching issue is also researched. There was little change in the spectrum after continuous ultrasound in a long time (**Figure S7),** which suggest that only few dyes leak out from the nanoparticles.

Magnetism

Owing to nanoscopic magnetic Fe_3O_4 contained into Fe_3O_4/DPPBPA@F-127 NPs, they are expected to be magnetically susceptible. **Figure 4** shows the plots of magnetization versus applied magnetic field at 300 K for OA-Fe_3O_4 and Fe_3O_4/DPPBPA@F-127. With the increasing of the magnetic field strength (Maximum filed=18000G), the magnetization of Fe_3O_4/DPPBPA@F127 swiftly increases and ultimately reaches a saturation magnetization (M_s) of 35.66 emu/g. There is no hysteresis and both remanence (M_r=0.3186emu/g) and coercivity (H_{ci}=6.377G) are nearly zero, which indicates that the NPs are superparamagnetic[46]. It should be noted that the saturation magnetization often reduce when the iron oxide was cladded in some matrix. Although the Ms value of Fe_3O_4/DPPBPA@F127 is a little bit lower than that of OA- Fe_3O_4 (M_s= 55.629 emu/g), the magnetization of Fe_3O_4/DPPBPA@F127 is already superior to those NPs reported previously.

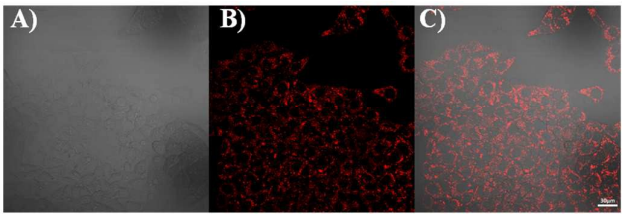

Figure 6. Confocal laser scanning microscopy images of MCF-7 cells after incubation with Fe_3O_4/DPPBPA@F127 for 6h at 37 ℃. A: bright field image; B: fluorescence image; C: overlay of A and B. AEE NPs Concentration: 50ppm. Scale bar for all images =30μm.

Next we explore the magnetic resonance imaging (MRI) ability of the NPs, due to the excellent magnetic characters of Fe_3O_4/DPPBPA@F127. Normally, with the same imaging parameters, the higher concentration of the contrast agent is the larger change of water relaxation in tissue. The spinlattice relaxation time T_1 of Fe_3O_4/DPPBPA@F127 NPs with different concentration of Fe_3O_4 loading in water was performed. From **Table 1**, we can know that $1/T_1$ increases with increasing the concentration of Fe_3O_4 from 1 mg to 2 mg. **Figure 5** shows the compartion of the T_1 contrast MRI image of water without and with the presence of Fe_3O_4/DPPBPA@F127 NPs carried out *in vitro* MRI experiments. It can be clearly observed that the different MRI contrast between map A and B, where the

View Article Online
DOI: 10.1039/C6RA07520G

contrast for map A, which is made with pure water, is fairly poor, whereas that for map B, which contain the Fe_3O_4/DPPBPA@F127 NPs, is much better**.** The contrast with the presence of Fe_3O_4/DPPBPA@F127 is significantly enhanced, suggesting the effective MRI ability.

Intracellular Imaging

The cytotoxicity of Fe_3O_4/DPPBPA@F-127 in the MCF-7 cells was studied by using 3-(4, 5-dimetylthiazol-2-yl)-2, 5-diphenyltetrazolium bromide (MTT) assay. **Figure S8** shows the cell viability after incubation with the NPs suspension at concentrations of 0, 5, 10, 20, 40, 60, 80, 100 ppm for 24 h, respectively. It was observed that cell viabilities for all the fluorogen concentrations within the tested periods of time were more than 95%, indicating that the Fe_3O_4/DPPBPA@F-127 NPs had low cytotoxicity or good biocompatibility. The low cytotoxicity makes the NPs promising for bioimaging applications and superior to QDs, which are well-known for their concentration-dependent cytotoxicity.

The in vitro cellular imaging of Fe_3O_4/DPPBPA@F-127 was performed by using confocal laser scanning microscopy (CLSM) with a 405 nm laser excitation and the fluorescent signals were collected at 620nm – 680nm to monitor the cell uptake behaviour to the NPs. Previous studies have showed that the FSNPs could selectively stain the cytoplasmic regions of the living cells. Phagocytosis may be the possible mechanism for intracellular uptake of the NPs. The NPs were enclosed by the cell membrane to form small vesicles, which were then internalized by the cells. The NPs were further processed in endosomes and lysosomes and are eventually released into the cytoplasm. As shown in **Figure 6**, after incubating with 50 ppm of Fe_3O_4/DPPBPA@F-127 for 6 h at 37 °C in the culture medium, an intense red fluorescence was observed in the cellular cytoplasms, which suggested the intracellular uptake of the NPs. These results manifested that the Fe_3O_4/DPPBPA@F-127 NPs were effective FR/NIR fluorescent bioprobes for cellular imaging with a high fluorescence contrast.

Conclusions

In summary, we succeeded in developping a simple strategy to fabricate multifunctional polymer NPs Fe_3O_4/DPPBPA@F-127, by using oleic acid coated magnetic Fe_3O_4 and an AEE molecule DPPBPA as the core, and biocompatible polymer Pluronic F-127 as the encapsulation matrix. The structure, morphology, and property of the NPs are characterized and investigated. The fluorescent magnetic NPs could be successfully dispersed in aqueous solution and showed significantly near-infrared emission (654nm) with high fluorescence quantum yields (18.3%). The high quantum yield of the fluorescent magnetic NPs are attributed to the restricted intramolecular rotation of the DPPBPA molecules in the spatially confined hydrophobic core environment of the NPs, which prevents direct interactions of DPPBPA molecules. The NPs are magnetically susceptible with zero remanence and coercivity, suggesting that they are good superparamagnets with high magnetization, which show effective MRI ability. The Fe_3O_4/DPPBPA@F-127 NPs show less cytotoxicity in aqueous solution, suggesting NPs are biocompatible nanocarriers. Due to its high brightness, low cytotoxicity and excellent stability, the obtained NPs have been successfully utilized in in vivo fluorescence imaging with high fluorescence contrast. We anticipate that this strategy of multifunctional NPs will inspire the development of a novel biological nanomaterials with high efficient fluorescence and strong magnetic susceptibility.

Experimental Section

Materials

All reagents and starting materials are commercially available and were used without further purification, unless otherwise noted. 1, 4-dibromo-2, 5-dimethylbnzene was purchased from Aladdin (Shanghai, China). Benzyl cyanide was purchased from J&K Scientific Ltd (Beijing China). Pluronic F-127 and MTT were purchased from Sigma–Aldrich (St. Louis, USA). Deionized water (18.2 MΩ·cm resistivity) from a Milli-Q water system was used throughout the experiments before being used as solvents.

Instrumentations

Mass spectra were recorded on an Agilent 1100 LC-MS system. ^{1}H NMR spectra were recorded on Bruker AVANVE 500 MHz spectrometer or Varian 300 MHz with tetramethylsilane as the internal standard. UV-vis absorption spectra were recorded using a Shimadzu UV-3600 UV-vis spectrophotometer. Solid state PL efficiencies were measured using an integrating sphere (C-701, Labsphere Inc.) with a 365 nm Ocean Optics LLS-LED as the excitation source, and the laser was introduced into the sphere through the optical fiber. Photoluminescence spectra were collected on a Shimadzu RF-5301PC spectrophotometer. DLS and Zeta potential measurement was performed using a Malvern Zetasizer Nano ZS size analyser at room temperature. Transmission electron microscopy (TEM) images were obtained using a transmission electron microscope (TEM, JEM-2100F). The cellular imaging was performed on an Olympus IX71 microscope with Mercury lamp as the excitation source.

Measurements of fluorescence quantum yields： Fluorescence quantum yields for the solutions and suspensions were obtained by comparing to the fluorescence spectrum of rhodamine in ethanol (absorbance value < 0.1, excitation wavelength:365 nm, PL efficiencies Φ_r= 69%) with corrections of refractive index differences using eqn[47].

$$\Phi_s = \Phi_r \left(\frac{A_r}{A_s}\right)\left(\frac{I_s}{I_r}\right)\left(\frac{n_s^2}{n_r^2}\right)$$

Where Φ_r and Φ_s are the fluorescence quantum yields of standards and the samples, respectively. A_r and A_s are the absorbances of the standards and the measured samples at the excitation wavelength, respectively. I_r and I_s are the

View Article Online
DOI: 10.1039/C6RA07520G

integrated emission intensities of standards and the samples. nr and ns are the refractive indices of the corresponding solvents of the solutions, respectively.

Measurements of the leaching issue

The leakage degrees of the dye in the matrix were investigated using fluorescence spectra. After continuous vigorous sonicating, Fe_3O_4/DPPBPA@F-127 NPs were separated by magnet from 1mL aqueous solution and then dispersed in 1mL water by sonicator. After that, the fluorescence was measured.

Synthesis of 2,5-Dibromobenzene-1,4-dicarbaldehyde (1)

2,5-Dibromobenzene-1,4-dicarbaldehyde (1) was synthesized according to the procedure shown in Scheme S1. All chemicals were purchased commercially, and used without further purification. 4g of 1, 4-dibromo-2, 5-dimethylbnzene was dissolved in 20 mL of acetic acid and 40 mL of acetic anhydride at 0 °C. 14 mL of sulfuric acid was added dropwise into the solution, which was stirred for another 10 min. CrO3 was grinded into powders, and then added to the mixture in portions. The resulting mixture was stirred vigorously for another 5 h at the temperature under 10°C.38 The greenish slurry was poured into ice water and filtered. The solid was washed with water and microscale cold methanol. The white compound would be get. The diacetate was then hydrolyzed by refluxing with a mixture of 20mL of water, 20 mL of ethyl alcohol, and 2 mL of sulfuric acid for 5 h. After the mixture cooled, the pale yellow product was separated by filtration. The crude product was purified by recrystallization from chloroform. Yellow crystal will be get(1.83g, 40%). 1 H NMR δ H (500 MHz, CDCl3) 10.38 (2 H, s), 8.19 (2 H, s).

Synthesis of (2Z,2'Z)-3,3'-(2,5-dibromo-1,4-phenylene)bis(2-phenylacrylonitrile) (2)

The mixture of benzylcyanide (201 mg, 1.5 mmol) and compound 1 (659 mg, 3 mmol) in tert-butyl alcohol (10 mL) was stirred at 46 °C for 30 min. Then, potassium tert-butoxide (1 M solution in tetrahydrofuran, 0.25 mL) and Tetrabutylammonium hydroxide (TBAH, 1 M solution in methanol, 0.25 mL) were slowly added, and stirred for 60 minutes[37]. The resulting precipitate was filtered and purified by column chromatography using dichloromethane. Compound 2 (348 mg) was obtained in yield of 70% by evaporated the solvent. ^{1}H NMR: δ_H (500 MHz, $CDCl_3$) 8.39 (2 H, s), 7.79 (2 H, s), 7.77 (4 H, dd, *J* 7.9, 1.2), 7.56 – 7.43 (6 H, m).

Synthesis of (2Z, 2'Z)-3, 3'-(2, 5-di(piperidin-1-yl)-1, 4-phenylene) bis(2-phenylacrylonitrile) (DPPBPA)

A vial tube (25 mL) equipped with a magnetic stirring bar was charged with $Pd_2(dba)_3$ (2.06mg, 22.5μmol) and Ruphos (42mg, 90μmol). The vial tube was then capped with a rubber septum, evacuated for 5 min and charged with nitrogen. The evacuation –purge operation was repeated twice. Toluene (10 mL) was added to the vial at room temperature under a nitrogen atmosphere and the resulting mixture was stirred at room temperature for 5 min. To the solution were added compound 2 (0.147 g, 0.3mmol), piperidine (0.297mL, 3mmol), and K_3PO_4 (0.87g, 3mmol)[48]. The mixture was stirred at 100°C for 15 h and then allowed to cool to room temperature. The reaction mixture was passed through a short pad of neutral alumina (activated level I). The filtrate was concentrated by evaporation. Then the crude product was purified by silica gel chromatography (hexane/CH_2Cl_2=1:1) to give a red solid. Then, the pure product was obtained by sublimation in the yield of 15%. ^{1}HNMR: δ_H (500 MHz, $CDCl_3$) 8.06 (2 H, s), 7.93 (2 H, s), 7.78 (4 H, d, *J* 7.6), 7.51 (4 H, t, *J* 7.6), 7.43 (2 H, t, *J* 7.4), 3.06 – 2.93 (8 H, m), 1.80 – 1.71 (8 H, m), 1.62 (4 H, s), GC-MS: $C_{34}H_{34}N_4$, calcd 498.66; found 498.66.

Synthesis of oleic acid coated Fe_3O_4

A solution of 0.01 mol ferric chloride hexahydrate and 0.005 mol ferrous chloride tetrahydrate in 100 mL of de-ionized (DI) water in a 3-neck round bottom flask was stirred by mechanical stirrer at 80 ºC with nitrogen bubbling for 30 min. 0.01 mol of potassium oleate was added, and the mixture was stirred for another 30 min. 35 mL of 4% ammonium hydroxide was added to the mixture. The reaction system turned to black immediately. The reaction continued at 80 ºC under nitrogen bubbling for 30 min. The black liquid was centrifuged at 60000r/min for 20min at 20 ºC to separate unreacted oleic acid from magnetic NPs. The magnetic NPs were dispersed in THF at 10 mg/mL for further application.

Preparation of Fe_3O_4/DPPBPA@F-127

In a typical preparation, the fluorescent DPPBPA was first dissolved in tetrahydrofuran (THF) to make a 0.5 mg/mL stock solution. OA-Fe_3O_4 (1mg, 2mg), DPPBPA (0.5mg, 1mg) and Pluronic F-127 (6mg, 8mg, 10mg, 12 mg) with different contentions were dispersed in 5mL THF by a vigorous bath sonicator. The solution mixture was quickly added to DI water, and the THF was removed by nitrogen stripping in a vigorous bath sonicator. The solution was concentrated by continuous nitrogen on a 90 ºC hotplate followed by filtration through a 0.2 micron filter. During nanoparticle formation, the OA-Fe_3O_4 and DPPBPA tended to entangled with the hydrophobic domains of Pluronic F-127, to afford the hydrophobic interiors, while the hydrophilic domains of Pluronic F-127 extend into the aqueous phase of the NPs.

Cell Culture

MCF-7 breast cancer cells were provided by American Type Culture Collection (ATCC). The cells were cultured in DMEM medium containing 10% heat-inactivated FBS (Invitrogen), 100 U/ml penicillin, and 100 μg/ml streptomycin (Thermo Scientific) and maintained in a humidified incubator at 37℃ with 5% CO_2. Before experiment, the cells were precultured until confluence was reached. MCF-7 cells were seeded in a 96-well flat-bottomed microplate (10000 cells/well) and cultured in 100 μL growth medium at 37℃ and 5% CO_2 for 24h. Cell culture medium in each well was then replaced by 100μL cell growth medium, containing Fe_3O_4/DPPBPA@F-127 with concentrations ranging from 0 to 100ppm. After incubation for 20h, 20μL of MTT (5mg/mL in PBS solution) was added to each well, and cells were incubated further for 4h at 37°C. The growth medium was removed gently, and 150 μL of DMSO was then added to each well, sitting at room

View Article Online
DOI: 10.1039/C6RA07520G

temperature overnight to dissolve the formazan crystals completely. The absorbance at the wavelength of 570 nm was measured by Multiskan EX (Thermo Electron Corporation), and each data point represents a mean +SD from triplicate wells.

Percentage cell viability = (average Abs value of experimental group - average Abs value of blank group) / (average Abs value of control group - average Abs value of blank group) ×100 %.

Percentage cell cytotoxicity = [1- (average Abs value of experimental group - average Abs value of blank group) / (average Abs value of control group - average Abs value of blank group)] ×100 %.

Percentage cell cytotoxicity = (1- Percentage cell viability) ×100 %.

Cell imaging

To study the cellular uptake, MCF-7 cells were added to 6-well plate, treated with various concentrations Fe_3O_4/DPPBPA@F-127 (50ppm) for 12 h. The cells were washed with PBS before observations on fluorescence microscopy. The cellular imaging was performed on a Fluorescence microscope. Cellular uptake of the NPs was investigated by using flow cytometer (FACS Calibur, Becton and Dickinson Company) with excitation and emission wavelengths of 460 nm and FLA-3. In total, 10,000 cells were analyzed per sample.

Acknowledgements

This work was supported by (2013CB834701), the Natural Science Foundation of China (No. 51373063, 51573068, 21221063) and Program for Chang Jiang Scholars and Innovative Research Team in University (No. IRT101713018).

Notes and references

1 M.-M. Titirici, M. Antonietti and A. Thomas, *Chemistry of Materials*, 2006, **18**, 3808-3812.
2 C. B. Murray, D. J. Norris and M. G. Bawendi, *Journal of the American Chemical Society*, 1993, **115**, 8706-8715.
3 L. Levy, Y. Sahoo, K.-S. Kim, E. J. Bergey and P. N. Prasad, *Chemistry of Materials*, 2002, **14**, 3715-3721.
4 J. M. Perez, T. O'Loughin, F. J. Simeone, R. Weissleder and L. Josephson, *Journal of the American Chemical Society*, 2002, **124**, 2856-2857.
5 P. S. Doyle, J. Bibette, A. Bancaud and J.-L. Viovy, *Science*, 2002, **295**, 2237.
6 T. Sen, A. Sebastianelli and I. J. Bruce, *Journal of the American Chemical Society*, 2006, **128**, 7130-7131.
7 K. Yang, L. Hu, X. Ma, S. Ye, L. Cheng, X. Shi, C. Li, Y. Li and Z. Liu, *Advanced Materials*, 2012, **24**, 1868-1872.
8 D. W. Hwang, I. C. Song, D. S. Lee and S. Kim, *Small*, 2010, **6**, 81-88.
9 X. Li, H. Li, G. Liu, Z. Deng, S. Wu, P. Li, Z. Xu, H. Xu and P. K. Chu, *Biomaterials*, 2012, **33**, 3013-3024.
10 W. Wang, Y. Xu, D. I. C. Wang and Z. Li, *Journal of the American Chemical Society*, 2009, **131**, 12892-12893.
11 S. Gai, P. Yang, C. Li, W. Wang, Y. Dai, N. Niu and J. Lin, *Advanced Functional Materials*, 2010, **20**, 1166-1172.
12 F. Mahtab, Y. Yu, J. W. Y. Lam, J. Liu, B. Zhang, P. Lu, X. Zhang and B. Z. Tang, *Advanced Functional Materials*, 2011, **21**, 1733-1740.
13 X. Brokmann, J. P. Hermier, G. Messin, P. Desbiolles, J. P. Bouchaud and M. Dahan, *Physical Review Letters*, 2003, **90**, 120601.
14 R. Naccache, F. Vetrone, V. Mahalingam, L. A. Cuccia and J. A. Capobianco, *Chemistry of Materials*, 2009, **21**, 717-723.
15 Y. Hong, J. W. Y. Lam and B. Z. Tang, *Chemical Society Reviews*, 2011, **40**, 5361-5388.
16 S. Zhang, J. Yan, A. Qin, J. Sun and B. Tang, *Sci. China Chem.*, 2013, **56**, 1253-1257.
17 Y. Dong, B. Xu, J. Zhang, X. Tan, L. Wang, J. Chen, H. Lv, S. Wen, B. Li, L. Ye, B. Zou and W. Tian, *Angewandte Chemie International Edition*, 2012, **51**, 10782-10785.
18 J. He, B. Xu, F. Chen, H. Xia, K. Li, L. Ye and W. Tian, *The Journal of Physical Chemistry C*, 2009, **113**, 9892-9899.
19 X. Li, S. Zhu, B. Xu, K. Ma, J. Zhang, B. Yang and W. Tian, *Nanoscale*, 2013, **5**, 7776-7779.
20 B. Zhou, H. Shan, D. Li, Z.-B. Jiang, J.-S. Qian, K.-S. Zhu, M.-S. Huang and X.-C. Meng, *Magnetic Resonance Imaging*, 2010, **28**, 394-399.
21 C. G. Khoury and T. Vo-Dinh, *The Journal of Physical Chemistry C*, 2008, **112**, 18849-18859.
22 A. Narita, K. Naka and Y. Chujo, *Colloids and Surfaces A: Physicochemical and Engineering Aspects*, 2009, **336**, 46-56.
23 Z. Wu, J. Huang and Y. Yan, *Langmuir*, 2015, **31**, 7926-7933.
24 Y. Li, H. Yu, Y. Qian, J. Hu and S. Liu, *Advanced Materials*, 2014, **26**, 6734-6741.
25 Y. Chen, M. Li, Y. Hong, J. W. Y. Lam, Q. Zheng and B. Z. Tang, *ACS Applied Materials & Interfaces*, 2014, **6**, 10783-10791.
26 K. Li, D. Ding, C. Prashant, W. Qin, C.-T. Yang, B. Z. Tang and B. Liu, *Advanced Healthcare Materials*, 2013, **2**, 1600-1605.
27 K. Justin Thomas, J. T. Lin, M. Velusamy, Y. T. Tao and C. H. Chuen, *Advanced Functional Materials*, 2004, **14**, 83-90.
28 M. A. Wolak, J. Delcamp, C. A. Landis, P. A. Lane, J. Anthony and Z. Kafafi, *Advanced Functional Materials*, 2006, **16**, 1943-1949.
29 G. Ulrich, R. Ziessel and A. Harriman, *Angewandte Chemie International Edition*, 2008, **47**, 1184-1201.
30 X. Zhang, M. Liu, B. Yang, X. Zhang, Z. Chi, S. Liu, J. Xu and Y. Wei, *Polymer Chemistry*, 2013, **4**, 5060-5064.
31 C.-K. Lim, S. Kim, I. C. Kwon, C.-H. Ahn and S. Y. Park, *Chemistry of Materials*, 2009, **21**, 5819-5825.
32 Z. Wang, L. Yan, L. Zhang, Y. Chen, H. Li, J. Zhang, Y. Zhang, X. Li, B. Xu, X. Fu, Z. Sun and W. Tian, *Polymer Chemistry*, 2014, **5**, 7013-7020.
33 B.-K. An, S.-K. Kwon, S.-D. Jung and S. Y. Park, *Journal of the American Chemical Society*, 2002, **124**, 14410-14415.
34 X. Y. Shen, W. Z. Yuan, Y. Liu, Q. Zhao, P. Lu, Y. Ma, I. D. Williams, A. Qin, J. Z. Sun and B. Z. Tang, *The Journal of Physical Chemistry C*, 2012, **116**, 10541-10547.
35 Y.-T. Lee, C.-L. Chiang and C.-T. Chen, *Chemical Communications*, 2008, 217-219.
36 36. Y. Liu, X. Tao, F. Wang, X. Dang, D. Zou, Y. Ren and M. Jiang, *The Journal of Physical Chemistry C*, 2008, **112**, 3975-3981.
37 Y. Xu, H. Zhang, F. Li, F. Shen, H. Wang, X. Li, Y. Yu and Y. Ma, *Journal of Materials Chemistry*, 2012, **22**, 1592-1597.
38 M. Shimizu, Y. Takeda, M. Higashi and T. Hiyama, *Angewandte Chemie*, 2009, **121**, 3707-3710.
39 B. Olle, S. Bucak, T. C. Holmes, L. Bromberg, T. A. Hatton and D. I. C. Wang, *Industrial & Engineering Chemistry Research*, 2006, **45**, 4355-4363.
40 J.-J. Lin, J.-S. Chen, S.-J. Huang, J.-H. Ko, Y.-M. Wang, T.-L. Chen and L.-F. Wang, *Biomaterials*, 2009, **30**, 5114-5124.
41 C. Wu, S. J. Hansen, Q. Hou, J. Yu, M. Zeigler, Y. Jin, D. R. Burnham, J. D. McNeill, J. M. Olson and D. T. Chiu, *Angewandte Chemie International Edition*, 2011, **50**, 3430-3434.

View Article Online
DOI: 10.1039/C6RA07520G

42 Y. Zhang, K. Chang, B. Xu, J. Chen, L. Yan, S. Ma, C. Wu and W. Tian, *RSC Advances*, 2015, **5**, 36837-36844.
43 L. Yuan, W. Lin, K. Zheng and S. Zhu, *Accounts of Chemical Research*, 2013, **46**, 1462-1473.
44 J. Zhao, K. Xu, W. Yang, Z. Wang and F. Zhong, *Chemical Society Reviews*, 2015, **44**, 8904-8939.
45 T. D. Ashton, K. A. Jolliffe and F. M. Pfeffer, *Chemical Society Reviews*, 2015, **44**, 4547-4595.
46 S. Sun, H. Zeng, D. B. Robinson, S. Raoux, P. M. Rice, S. X. Wang and G. Li, *Journal of the American Chemical Society*, 2004, **126**, 273-279.
47 S. R. Forrest, *Nature*, 2004, **428**, 911-918.
48 M. Shimizu, R. Kaki, Y. Takeda, T. Hiyama, N. Nagai, H. Yamagishi and H. Furutani, *Angewandte Chemie International Edition*, 2012, **51**, 4095-4099.

View Article Online
DOI: 10.1039/C6RA07520G

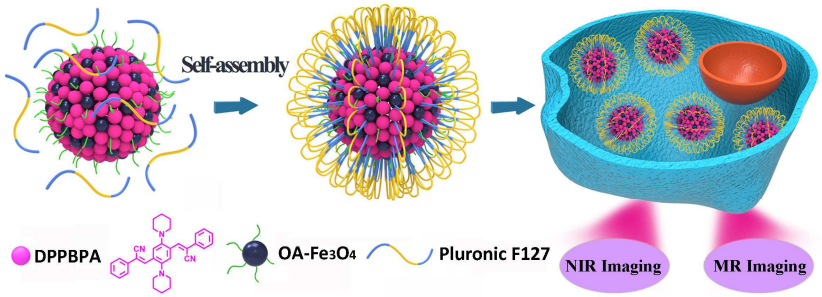

Magnetic fluorescent multifunctional polymer NPs Fe_3O_4/DPPBPA@F-127 and their application in MRI and NIR imaging.